Supporting Information

Cheng et al. 10.1073/pnas.1014995108

SI Text

Atomic Model Building and Refinement. The cryo-EM map at 3.9 Å shows clear backbones and side chains and is good enough for full atomic model building. Initial polyalanine models for each conformer were built manually using Coot (1). Large residues (Trp, Tyr, Phe, Arg, and His) were then assigned to the density map according to side chain density. The credibility of these residues was further confirmed by comparing the residue number between each adjacent large residue in the models with the protein sequences. Finally, all other residues were assigned using these large residues as a reference. Each of the residues was further verified according to side chain electron density.

Real-space electron density maps were segmented and put into artificial crystal lattices in space group P1 for each of the five structures and then converted to reciprocal space to generate simulated crystallographic diffraction data. The models were then refined in a pseudocrystallographic manner using Crystallography and NMR System (CNS) (2) within the resolution range 50–4.0 Å for VP3 and 50–3.9 Å for the other structures. The procedure included simulated annealing refinement, crystallographic conjugate gradient minimization, and group B-factor refinement, using maximum likelihood refinement targets with amplitude and phase probability distribution. Some errors in the model not resolved by automatic refinement were corrected manually in Coot and then refined again by CNS. The commonly used crystallographic refinement is an iterative improvement of electron density maps and models, but this pseudocrystallographic refinement procedure was used to correct the atomic model only, not to modify the density map. So during each cycle of refinement, the starting amplitudes and phases were always the original ones converted from the reconstructed electron density map, rather than from the previous cycle of pseudocrystallographic refinement. The geometry of the models was validated by PROCHECK (3) and MOLPROBITY (4). Refinement statistics are given in Table S1.

1. Emsley P, Cowtan K (2004) Coot: Model-building tools for molecular graphics. *Acta Crystallogr D* 60:2126–2132.
2. Brunger AT, et al. (1998) Crystallography & NMR system: A new software suite for macromolecular structure determination. *Acta Crystallogr D* 54:905–921.
3. Laskowski RA, Moss DS, Thornton JM (1993) Main-chain bond lengths and bond angles in protein structures. *J Mol Biol* 231:1049–1067.
4. Davis IW, et al. (2007) MolProbity: All-atom contacts and structure validation for proteins and nucleic acids. *Nucleic Acids Res* 35:W375–W383.

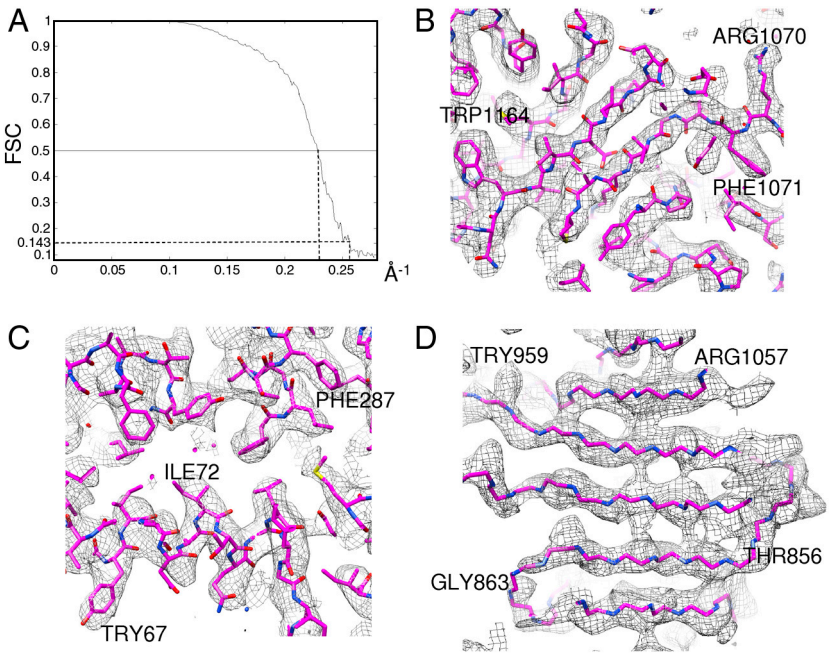

Fig. S1. Fourier shell correlation (FSC) and superimpositions of cryo-EM densities on their models demonstrate the effective resolution. Some residues are labeled. (*A*) Fourier shell correlation curve. The estimated resolution of the cytoplasmic polyhedrosis virus (CPV) capsid was 4.3 Å at FSC = 0.5 and 3.9 Å at FSC = 0.143. (*B*) β-strands in VP1B. (*C*) α-helix in VP5A. (*D*) Region (β-strands) of VP3 at outermost radius. It shows that the backbone is still traceable although those side chains were not resolved well.

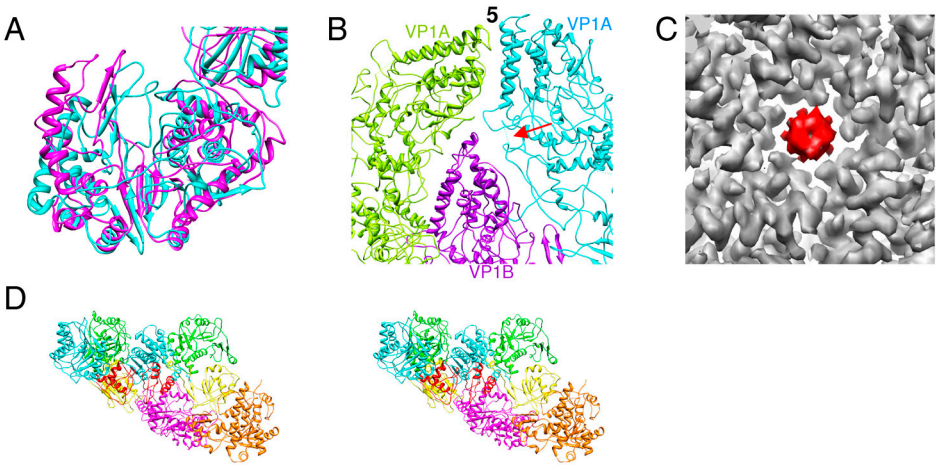

Fig. S2. Pathway for mRNA capping. (*A*) Zoom-in view of part of Fig. 3*B* (*Left*). Guanylyltransferase (GTase) domain of CPV VP3 (magenta) is superimposed on the counterpart in orthoreovirus λ2 (cyan). It shows that the structural topology of the CPV VP3 GTase domain is conserved with its counterpart in orthoreovirus. (*B*) The red arrowhead points to a proposed mRNA channel on the inner shell formed by two copies of VP1A and a copy of VP1B. Fivefold axis is marked with "5." (*C*) The pentameric channel formed by five copies of VP1A connecting the inner capsid chamber and the turret cavity is blocked by a strong nodule-like density (red). (*D*) Stereo view of two copies of VP3 [copy A (*Left*); copy B (*Right*)]. They have the same orientations as those in Fig. 3*C*. The GTase domains in copy A and copy B are colored with magenta and orange for clarity. The Bridge, Brace, methyltransferase-1 (MTase-1), and MTase-2 domains of both copies of VP3 (*A* and *B*) are labeled and colored in yellow, red, cyan, and green, respectively. A side channel is formed by two copies of brace domain (red).

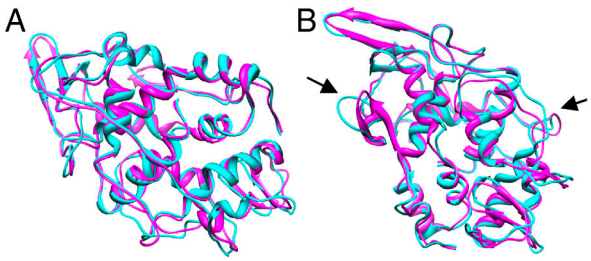

Fig. S3. Structural comparison between VP5A and VP5B. (*A*) Top view of superimposition of atomic models of VP5A (cyan) on VP5B (magenta) The top views of the two conformers are almost identical. (*B*) Bottom view of VP5A (cyan) and B (magenta). Arrowheads point their differences.

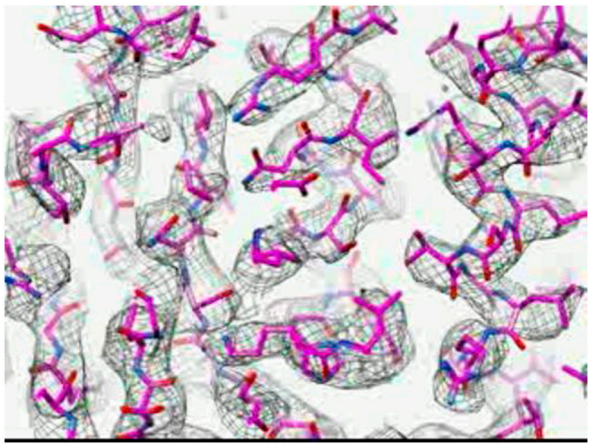

Movie S1. Rotational part view of superimposing the density map of VP1 on the atomic model. It shows that most side chains are fitted very well.
Movie S1 (MOV)

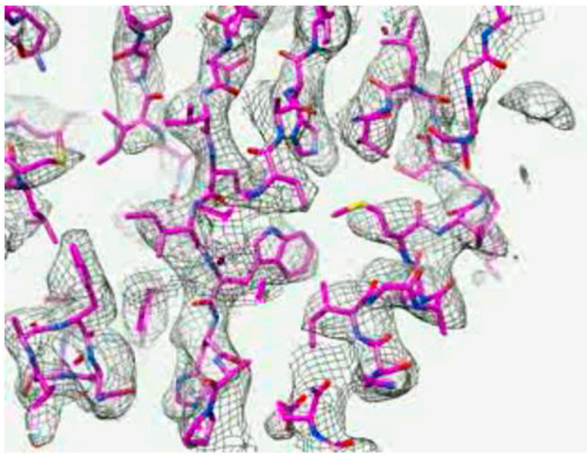

Movie S2. Rotational part view of superimposing the density map of VP3 on the atomic model. It shows that most side chains are fitted very well. Movie S2 (MOV)

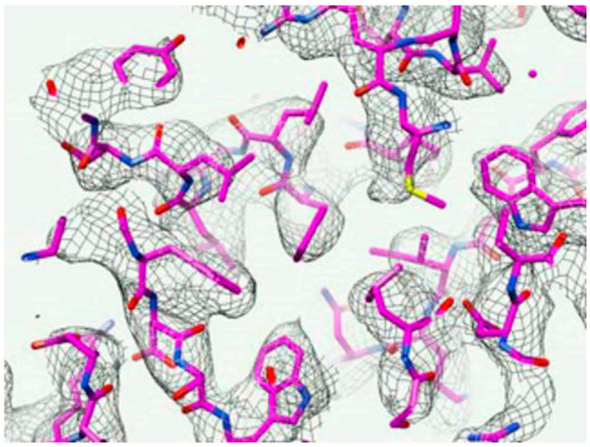

Movie S3. Rotational part view of superimposing the density map of VP5 on the atomic model. It shows that most side chains are fitted very well. Movie S3 (MOV)

Movie S4. Superimposing the atomic model of VP3 (magenta and red) on λ2 (cyan and blue). It shows that they have a very similar structural topology except that VP3 does not have the flap-like structure (blue) present on the top of the λ2 and VP3 has an extra "brace domain" (red).
Movie S4 (MOV)

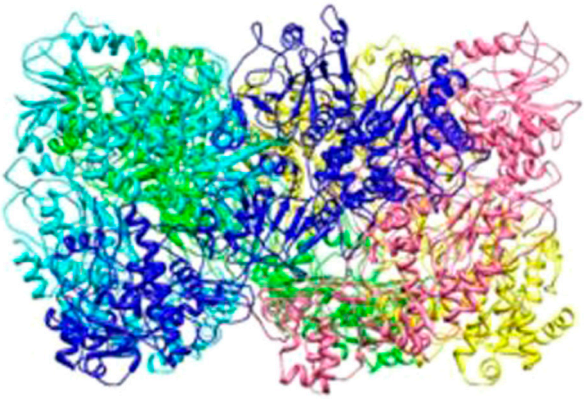

Movie S5. The organization of pentameric turret and the spike-like protein complex. Five copies of VP3 atomic models are shown in different colors and then the brace domains are colored in red. Surface view of the turret shows the mRNA channel connecting the GTase and MTase regions.
Movie S5 (MOV)

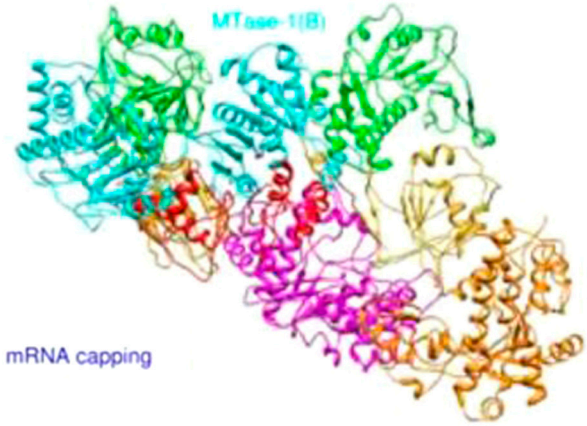

Movies S6. It shows how the enzymatic domains are arranged in two copies of VP3. The color code is the same as that of Fig. 3*C*.
Movie S6 (MOV)

Table S1. Refinement statistics

	VP1A	VP1B	VP3	VP5A	VP5B
Cell dimension (Å)*	238.00	214.20	142.80	76.16	85.68
Resolution range (Å)	50–3.9	50–3.9	50–4.0	50–3.9	50–3.9
Reflection number	475889	346942	95411	15671	22149
Number of atoms	9318	9805	8348	2277	2277
R_{work}/R_{free}†	0.271/0.273	0.319/0.322	0.297/0.313	0.312/0.318	0.318/0.329
rmsd bond	0.011	0.014	0.012	0.010	0.010
rmsd angle	1.754	2.028	1.774	1.718	1.783
Ramachandran plot:					
Residues in allowed regions	98.1%	98.5%	93.9%	100%	100%
Residues in most favored regions	81.6%	81.9%	77.1%	88.6%	90.0%

*$a = b = c$, $\alpha = \beta = \gamma = 90°$.
†$R_{work} = \sum(||Fp(obs)| - k * |Fp(calc)||)/\sum|Fp(obs)|$, k is the scaling factor; R_{free} was calculated for 10% of reflections randomly excluded from the refinement.